The FEBS Journal

FEBS PRESS science publishing by scientists

STRUCTURAL SNAPSHOT

Structural snapshots of the cellular folded protein translocation machinery Bcs1

Di Xia

Laboratory of Cell Biology, National Cancer Institute, National Institutes of Health, Bethesda, MD, USA

Keywords
AAA protein; Bcs1; Complex III; Cryo-EM; cytochrome bc_1 complex; folded protein translocation; iron-sulfur protein; membrane protein; X-ray crystallography

Correspondence
D. Xia, Laboratory of Cell Biology, Center for Cancer Research, National Cancer Institute, NIH, Bethesda, MD 20892, USA
Tel: (240) 760 7241
E-mail: xiad@mail.nih.gov

(Received 14 July 2020, revised 5 September 2020, accepted 22 September 2020)

doi:10.1111/febs.15576

Proteins destined to various intra- and extra-cellular locations must traverse membranes most frequently in an unfolded form. When the proteins being translocated need to remain in a folded state, specialized cellular transport machinery is used. One such machine is the membrane-bound AAA protein Bcs1 (Bcs1), which assists the iron-sulfur protein, an essential subunit of the respiratory Complex III, across the mitochondrial inner membrane. Recent structure determinations of mouse and yeast Bcs1 in three different nucleotide states reveal its homo-heptameric association and at least two dramatically different conformations. The apo and ADP-bound structures are similar, both containing a large substrate-binding cavity accessible to the mitochondrial matrix space, which contracts by concerted motion of the ATPase domains upon ATP binding, suggesting that bound substrate could then be pushed across the membrane. ATP hydrolysis drives substrate release and resets Bcs1 conformation back to the apo/ADP form. These structures shed new light on the mechanism of folded protein translocation across a membrane, provide better understanding on the assembly process of the respiratory Complex III, and correlate clinical presentations of disease-associated mutations with their locations in the 3D structure.

Introduction

Protein translocation occurs when proteins are moved across membranes to various destinations inside and outside the cell, whereas protein dislocation takes place in the process of protein quality control and homeostasis. These two very important processes, despite requiring different cellular machinery, occur through a ubiquitous threading mechanism in which protein substrates are unfolded while being translocated. Examples of protein translocation apparatus are the SecY channel on the prokaryotic cytoplasmic membranes, the Sec61 channel of the endoplasmic reticulum (ER) membranes of eukaryotes [1], and the TOM and TIM23 complexes of mitochondria [2]. On the other hand, the human AAA unfoldase Cdc48/p97 is a well-established example of cellular protein dislocation machinery needed for protein quality control and homeostasis, including ER-associated degradation [2–4].

Not all proteins are transported in the same unfolded fashion. The transport of the mitochondrial Rieske iron-sulfur protein (ISP) across the inner membrane (IM) is a well-established example. The ISP is one of the three essential subunits of the mitochondrial

Abbreviations
AAA, ATPases associated with various cellular activities; Bcs1, bc1 synthesis 1; bcs1, yeast bcs1 gene; Bcs1, human bcs1-like protein; BCS1L, human bcs1-like gene; cyt bc_1, cytochrome bc1 complex or Complex III; cyt, cytochrome; IMS, mitochondrial intermembrane space; ISP, Rieske iron-sulfur protein; ISP-ED, extrinsic domain of ISP; mBcs1, mouse Bcs1 protein; pmf, proton motive force; Rip1, yeast iron-sulfur protein; RIP1, yeast iron-sulfur protein gene; ROS, reactive oxygen species; TM, transmembrane; yBcs1, yeast bcs1 protein.

respiratory Complex III, also known as the cytochrome bc_1 complex (cyt bc_1). As a mid-segment of the respiratory chain, Complex III couples the reaction of electron transfer from ubiquinol to cyt *c* to the proton translocation across the membrane, contributing to the mitochondrial proton motive force (pmf) [5,6]. Inhibition of Complex III has evolved as an effective survival strategy in the microbial world over the course of evolution and has been widely used for disease treatment in agriculture and in medicine [7]. The functional importance of Complex III is also exhibited by the fact that mutations in its components lead to various mitochondrial diseases [8]. Complex III of eukaryotic organisms is dimeric, each monomer consisting of 10 (*Saccharomyces cerevisiae*) or 11 (*Bos taurus*) different subunits [5,6]. All subunits of Complex III, except for cyt *b*, are nucleus-encoded, brought into the mitochondrial matrix and refolded before being integrated into Complex III [9,10]. The ISP subunit in particular requires additional assistance to cross the mitochondrial IM again, going into the intermembrane space (IMS) as folded protein. Bcs1 is a protein that plays a key role in assisting the ISP subunit to cross the mitochondrial IM [11].

A mature ISP subunit, as shown in the structure of Complex III, consists of two domains: an N-terminal transmembrane (TM) helix and a C-terminal, functional globular domain, also known as the ISP extrinsic domain (ISP-ED), which contains a 2Fe-2S cluster and is located in the IMS in the final assembled Complex III. A flexible yet highly conserved linker connects the two domains [12,13]. The integration process of ISP into Complex III of high eukaryotes such as the cow is slightly different from that of lower eukaryotes as in yeast. The maturation of the ISP precursor takes place in the mitochondrial matrix because of the matrix localization of the iron-sulfur cluster synthesis machinery [14]. Following its entry into the mitochondrial matrix as an unfolded polypeptide chain, the ISP precursor folds into an apoprotein amenable to 2Fe-2S cluster installation [15,16]. For the fully assembled ISP precursor, its functional C-terminal domain, ISP-ED, must be translocated again across the IM into the IMS, while its TM helix becomes associated with the membrane section of Complex III and the N-terminal long signal sequence remains in the matrix. After the integration is complete, the precursor of the mammalian ISP is processed in a single step, resulting in a mature ISP with the signal peptide retained as subunit 9 [16]. Yeast Rip1 (yeast ISP), however, requires a two-step process by mitochondrial processing peptidase and mitochondrial intermediate protease [16].

Identified initially in baker's yeast (*S. cerevisiae*) as a protein factor required for incorporation of Rip1 into the yeast Complex III [17,18], Bcs1 is a mitochondrial membrane protein consisting of a Bcs1-specific domain at its N terminus and an ATPase domain at its C-terminus, the latter bears sequence similarity to the ATPases associated with various cellular activities family proteins (AAA). AAA family members are involved in a wide range of essential cellular processes including protein quality control and sorting, DNA replication and repair, and membrane fusion [19]. Morphologically, they most frequently occur as ring-shaped homo-hexameric ATPases, forming a central pore for peptide threading or moving along DNA strand. Recent advances in structural studies of AAA proteins have unveiled a hand-over-hand or split washer threading mechanism common to these hexameric AAA proteins, in which coexisting, sequentially arranged nucleotide states in subunits of the hexamer are found coordinating with channel-forming substrate-engaging pore loops that are arranged in a spiral staircase-like fashion. Presumably, a cycle of sequential, around-the-ring ATP hydrolysis performed by the ATPase domains results in stepwise substrate translocation [3,20–24]. Whether the operation of Bcs1 follows the established principle of AAA protein function remains to be seen, given the fact that some of the critical residues in the pore loops of AAA proteins are not conserved in Bcs1 [11]. As an integral membrane protein, Bcs1 is anchored to the mitochondrial IM by single N-terminal TM helices of its subunits with most of the molecule remaining in the matrix [25]. Linkage of Complex III deficiencies to mutations in DNA identified the culprit to be human bcs1-like gene (*BCS1L*), the human ortholog of yeast bcs1 [26–28]. In addition to its requirement for Complex III assembly, Bcs1 was shown to also regulate the amount of Complex III in mitochondria in response to availability of fermentable carbon sources in yeast [29]. Despite the clear evidence of involvement of Bcs1 in Complex III assembly shown by genetic and biochemical studies, exactly how Bcs1 performs its function remains unclear. The recent reported structures of mouse (mBcs1) and yeast (yBcs1) Bcs1 shed new lights on the assembly of Complex III, mutations linked to Complex III deficiency, and the mechanism of function of a distinct family of AAA proteins [30,31].

Structure of apo Bcs1

Structures of the mBcs1 and yBcs1 in apo form were recently determined by Cryo-EM [30,31]. Because the

structures are similar in most aspects, the following discussion will be based largely on the mBcs1. References will be made if certain structural features are only observed in the yBcs1. Apo mBcs1 takes the form of a heptamer and, when viewed perpendicular to the 7-fold axis with the mitochondrial matrix at the bottom, has an overall shape of an upside-down mushroom (Fig. 1A,B). The heptameric arrangement of Bcs1 was also confirmed by crystal diffraction data, displaying a 7-fold symmetry axis in self-rotation function searches from both full-length and a AAA domain fragment crystals [30], indicating a deviation from the classic hexameric structure found in most AAA proteins [19]. The structure of apo mBcs1 can be divided into three regions: the AAA region, the Bcs1-specific region (also called the seal-forming region), and the TM region; each region is ~ 30–40 Å in length. Unique to the apo structure is the ~ 15 Å gap, called interstitial gap, between the Bcs1-specific region and the AAA region. The apo structure features two large cavities: One is referred to as the substrate-binding cavity, which is encircled by AAA and part of the Bcs1-specific domains of the subunits and the other is called the TM basket, which is formed by TM helices. The two cavities are separated by a protein layer made of residues from the Bcs1-specific region (Fig. 1C). At the center of the protein layer, there is a small pore connecting the two cavities, which is plugged by a piece of density of unknown identity.

The structure of the apo mBcs1 has only half of the TM helix modeled (PDB: 6UKP), whereas the yeast structure in the ADP state contains the entire TM helix (PDB: 6SH4), which measures ~ 50 Å in length and forms an angle of about 35° with the plane of the membrane (Fig. 1D). They contact each other on the IMS side of the membrane, but on the matrix side at the beginning of the Bcs1-specific domain two neighboring helices are separated by a 25 Å gap.

Interestingly, two apo forms have been observed for the yBcs1 based on cryo-EM 3D classification and refinement, which were referred to as Apo1 and Apo2 [31]. A notable difference between the Apo1 and Apo2 state was found in the Bcs1-specific domain. While the pore separating the substrate-binding cavity and TM basket domain in the Apo1 form is tightly sealed, that for Apo2 appears to be open [31].

Domain structures of Bcs1

Sequence alignment of Bcs1 from different eukaryotic organisms indicates identical domain organization of their subunits, consisting of an N-terminal mitochondrial targeting and sorting domain that includes a TM segment [25,26], a middle Bcs1-specific or seal-forming domain, and a C-terminal AAA ATPase domain (Fig. 2A).

The tertiary structure of the Bcs1-specific domain (Residues 49–165 of mBcs1) appears to be unique. A search of the protein structure database revealed no similar protein folds [32]. The Bcs1-specific domain includes two β-sheets (Fig. 2B): Four antiparallel strands A, F, E, and D contribute to Sheet I. Sheet II, formed by two antiparallel stands (B and C), is also called connector hairpin because it reaches down and interacts with a neighboring AAA domain (Fig. 1A). In addition, there are two helices (H1 and H2) that provide support for the two β-sheets. When associated in the heptamer, the Bcs1-specific region forms two layers when viewed along the 7-fold axis from the membrane (Fig. 2C). The Sheet I forms the top layer and Sheets II and the two helices are in the bottom layer. Furthermore, Sheet I joins Sheet II of its neighboring subunit to form a continuous six-stranded β-sheet, giving the entire Bcs1-specific region the appearance of a 7-bladed propeller. In addition, a loop between strands E and F, named the seal loop, protrudes toward the central axis of the heptamer, forming a small constriction ~ 5 Å in diameter (Fig. 2C).

The AAA ATPase domain has 254 residues (Residues 165–418 for mBcs1). In addition to the EM structure, the structure of the AAA domain alone was determined by X-ray crystallography at 2.2 Å resolution (PDB: 6U1Y). These structures contain features that are consistent with the analysis of yeast mutants and their revertants [33]. As in typical AAA domains, there are two subdomains: a large RecA-like domain and a small characteristic helical domain (Fig. 2D). At the interface between the two subdomains lies the nucleotide-binding site. Most interestingly, the structure reveals that the AAA domain of Bcs1 is unique in that it includes a 7-stranded β-sheet in the RecA-like subdomain, which is the first of its kind reported for a AAA protein (see below for more details about unique features in Bcs1).

For apo Bcs1, the heptameric association of Bcs1 subunits leads to creation of a large barrel-like cavity or substrate-binding cavity encircled by the AAA domains and part (Sheet II or connector hairpin and Helix 2) of the Bcs1-specific domains from the subunits. The barrel has a diameter of ~ 40 Å at its widest part and is capped by the rest (Sheet I and Helix I or seal-forming domain) of the Bcs1-specific region (Fig. 1C). A large entrance accessible to the matrix allows protein substrate to enter the cavity.

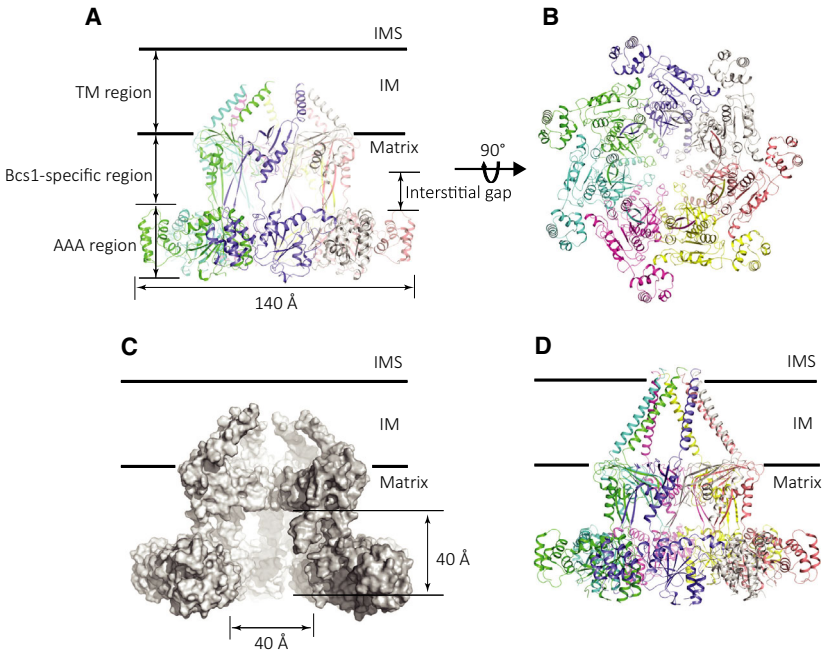

Fig. 1. Structure of mBcs1 in apo state. (A) Ribbon diagram of mBcs1 determined by cryo-EM in the absence of nucleotide viewed perpendicular to the 7-fold axis. The model is orientated with the IMS of the mitochondria at the top, and the matrix is at the bottom. The mitochondrial IM is indicated by the two parallel black lines. The TM helices are only partially visible from the EM density. The model is derived from PDB: 6UKP. All ribbon diagrams were rendered using the molecular graphics program PYMOL (http://pymol.org). (B) A 90-degree rotated view of mBcs1 model looking down the 7-fold axis. (C) Surface rendition of mBcs1 model with two of its subunits removed showing the large substrate-binding cavity, the TM cavity, or TM basket and the protein layer separating these two cavities. (D) Ribbon diagram of yBcs1 in the ADP-bound state as a comparison where models for TM helices are complete.

Conformational change revealed by the structure of mBcs1 with bound ATP

Isolated Bcs1 is enzymatically active. mBcs1 possesses the kinetic constants for ATP binding (K_m) of 0.04 mM and V_{max} of 5.8 nmol Pi/nmol protein/min [30]. The presence of ATP or its analogs in solution results in Bcs1 undergoing conformational change that can be detected by Blue-Native PAGE (BN-PAGE), causing a shift in the migration of the protein band. Interestingly, conformation of mBcs1 seems not to be affected by presence of ADP in solution, as no change was detectable in the migration of the protein in BN-PAGE. A similar observation was also previously reported for yeast Bcs1 [34].

When the structure of mBcs1 in the presence of ATPγS was first determined, a piece of density was found in the nucleotide-binding pocket of the AAA domain, which matches the shape and size of ATPγS (Fig. 2D). Both the EM density and the resulting AAA domain model were successful in phasing the diffraction data of a $^{\Delta N}$mBcs1 crystal that grew in the presence of AMP-PNP, yielding a high-resolution heptameric $^{\Delta N}$mBcs1 structure that shows clearly bound AMP-PNP (PDB: 6U1Y), indicating conformational similarity between the ATPγS- and AMP-PNP-bound Bcs1 [30].

Unlike the apo mBcs1, the TM region in the ATPγS state was not visible. Therefore, the first residue seen for this structure is I49 at the beginning of the Bcs1-specific domain. ATPγS binding drives mBcs1 to undergo a conformational transition when compared to the apo mBcs1. It resembles the shape of a bullet head morphologically, when viewed perpendicular to the 7-fold axis, and becomes more compact with a reduced barrel diameter (Fig. 3A,B). Although the binding of ATPγS seems to have minimal impact on the AAA domain as well as the Bcs1-specific domain in terms of structural changes, the binding does induce significant shifts in relative positions of the domains, thus altering how a subunit interacts with its neighboring subunits. Such changes can be clearly illustrated by superposing an ATPγS-bound subunit to an apo

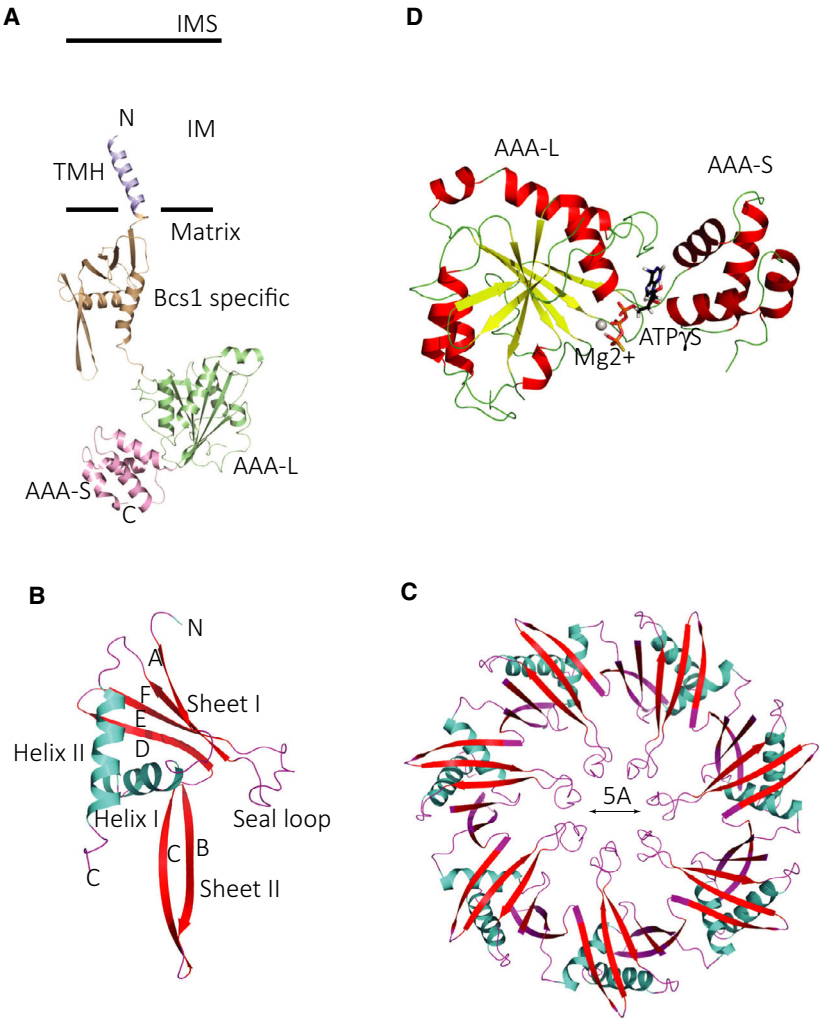

Fig. 2. Structures of Bcs1 domains: (A) Each Bcs1 subunit has three domains: the TM (purple), Bcs1-specific (brown), and AAA domains. The AAA domain is further divided into the AAA-large (AAA-L) in green and AAA-small (AAA-S) in magenta. The mitochondrial IM is indicated by the two parallel lines. (B) The Bcs1-specific domain has a novel fold, formed by two β-sheets (Sheet I and Sheet II) and two α-helices (Helix I and Helix II). (C) The heptameric association of the Bcs1-specific domain, viewed along the 7-fold axis from the matrix, allows formation of seven 6-stranded β-sheets, which is the structural basis for the seal. (D) The structure of the AAA domain consists of two subdomains: a large RecA-like domain, also called AAA-L, and a small helical domain, referred to as AAA-S. The AAA-L domain features a unique 7-stranded β-sheet. The ATPγS is shown as a stick model with carbon in black, oxygen in red, and sulfur in yellow. The Mg^{2+} ion is shown as a metallic ball.

subunit and observing the domain movement of the same subunit and relative changes in positions of the neighboring subunits (Fig. 3C). For example, by superposing the two AAA ATPase domains in different nucleotide states, one can observe a very large movement by the Bcs1-specific domain, where such a movement can be as large as 45 Å measured from the tip of the Helix II of the Bcs1-specific domain.

The largest conformational change by far that can be visualized is when mBcs1 subunits in ATPγS state are associated as heptamers, as the interstitial gap between the Bcs1-specific region and the AAA region disappears and the substrate-binding cavity collapses. For the apo mBcs1, the prominent feature is the barrel-shaped, very large substrate-binding cavity, which is accessible from the mitochondrial matrix. The barrel is ~ 40 Å in diameter at its widest point and runs as deep as 40 Å along the 7-fold axis (Fig. 3D). It has an estimated volume of ~ 28 000 $Å^3$, sufficient to contain a folded protein such as the C-terminal functional domain of ISP (ISP-ED, 126 residues, 21 000 $Å^3$). This cavity contracts dramatically when ATPγS binds, shrinking the widest part of the barrel by half to 20 Å and reducing its length to 25 Å. As a result, the volume of the cavity decreases to ~ 9000 $Å^3$ and therefore is no longer able to accommodate the folded ISP-ED (Fig. 3D).

The nucleotide dependence of the conformational change in the TM region is poorly defined, because structures in this region under both apo and ATP states were not well determined for mouse Bcs1. Nevertheless, a glimpse of the TM helix conformation of apo Bcs1 was obtained on the basis of the partially determined structure in that region of mBcs1 and the fully determined TM helices for the yBcs1 in ADP state (Fig. 1A,D). The direction of the partially determined TM helices in mBcs1 suggests close association at the IMS side of the TM helices in the apo structure,

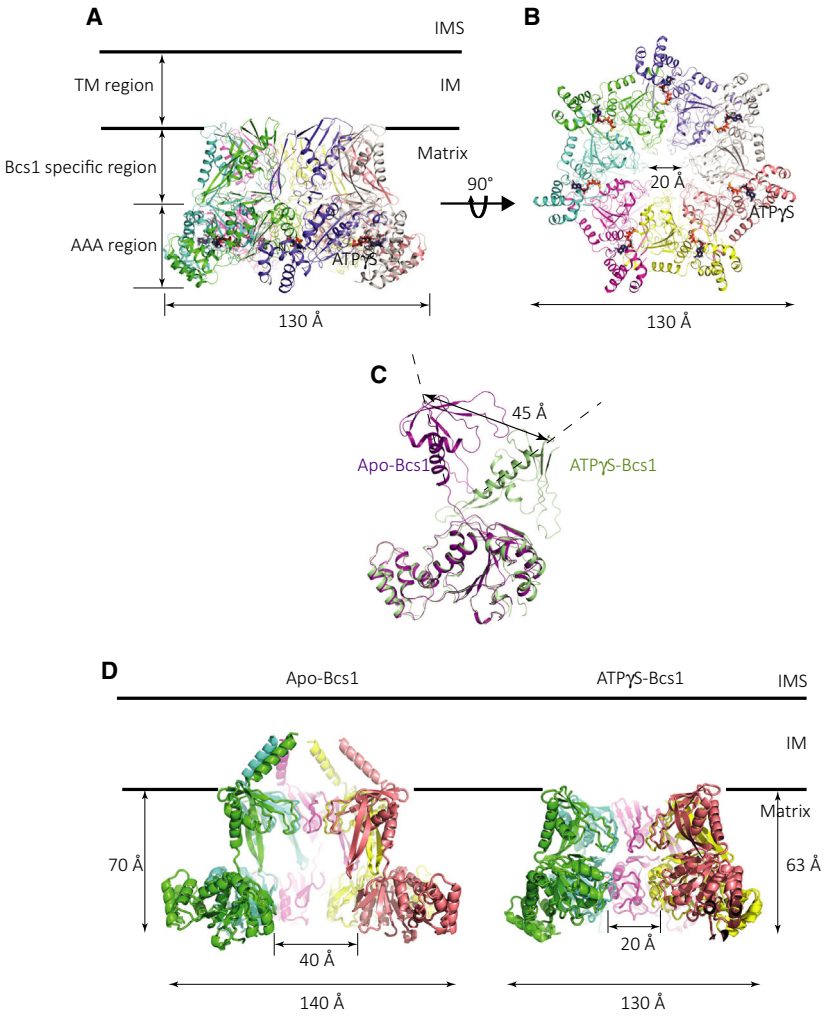

Fig. 3. Structure of mBcs1 in ATP state and conformational changes. (A) Ribbon diagram of the structure of heptameric mBcs1 with bound ATPγS viewed perpendicular to the 7-fold axis. The two horizontal parallel lines delineate the boundary of mitochondrial IM from the matrix and IMS as indicated. Seven ATPγS molecules are drawn as stick models and one of them is labeled. (B) 90-degree rotated view from the orientation in (A). Again, one ATPγS is labeled. (C) Superposition of AAA domains of Bcs1 subunits between ATPγS-bound (green) and apo (magenta) conformations. The positional movement of Helix II expressed as the distance change in residue K145 from the tip of the Helix II is indicated. (D) Collapsing of the substrate-binding cavity as Bcs1 transitions from the apo to the ATPγS-bound forms. On the left is the Apo-Bcs1 model with two subunits deleted to more easily view the Bcs1 interior. Similarly, cartoon rendition of the ATPγS-bound mBcs1 is given on the right, which has two of its subunits removed.

which is supported by the observation in the yBcs1 structure of fully ordered TM helices. On the other hand, TM helix conformation for the ATPγS-bound Bcs1 could not be clearly determined due to poor density and could only be guessed from the starting position of the residues in the Bcs1-specific domain, which was residue I49. The fact that the TM helices are disordered suggests a lack of interactions among the TM helices when ATP is bound, which seems consistent with the post-translocation conformation.

Structures of Bcs1 in ADP state

We began our structure determination of mBcs1 by crystallizing purified mBcs1 in the presence of ATPγS·Mg^{2+}, because biochemical studies suggested a more compact protein when mBcs1 and ATPγS·Mg^{2+} were present together in solution. We obtained crystals and a complete diffraction data set to 4.4 Å resolution. Surprisingly, we were able to determine and refine the structure by the molecular replacement method only when we used the coordinates of the apo mBcs1 as a phasing model. In contrast to the apo mBcs1, the nucleotide-binding pockets in the AAA domains of this structure were occupied by large pieces of density that could be modeled as bound ADP in standard geometry [30]. ADP binding induces only local changes in the vicinity of bound nucleotides, while the overall conformation of mBcs1 resembles that of apo mBcs1.

One of the reported yeast structures has ADP molecules that uniformly occupy the nucleotide-binding pockets of the AAA domains [31], which was the result of incubating the protein with ATP during sample preparation and likely represents an ADP-bound posthydrolysis ground state of the protomers (PDB: 6SH3). Consistent with the crystal structure of the mBcs1 in ADP state, the ADP-bound yBcs1 adopts the conformation of apo Bcs1.

Mechanistic insight concerning folded protein translocation across membranes by Bcs1

As early as 1992, the Bcs1 gene was identified in yeast, its product localized to the mitochondrial IM, and recognized as a requirement for ISP incorporation into Complex III, suggesting its ability to move the 15 kDa functional domain (ISP-ED) of the ISP subunit across the IM of mitochondria [17,35]. This hypothesis gained support by experiments showing that mutations causing partial unfolding of ISP failed to be transported by Bcs1 [34]. Because installation of the 2Fe-2S cluster into apo ISP occurs in the mitochondrial matrix, translocation of the ISP-ED going into the IMS in its folded form becomes mandatory. However, it is by no means trivial to move a 126-residue folded protein domain across the membrane barrier, giving its 25 Å diameter and the need to maintain a large pmf across the IM. Until the structure determination of Bcs1, cellular machinery facilitating passage of substrates of this size through the channel of a AAA protein had not been visualized [11]. By obtaining the mBcs1 and yBcs1 structures in three different nucleotide states and many conformations, we are now in a position to derive important insights into the mechanics of the transport process (Fig. 4). First, in order to transport a substrate, the size of the ISP-ED, the Bcs1 channel must be sufficiently large. Therefore, Bcs1 occurs in the form of a heptamer instead of a hexamer (the latter form is more frequently seen in AAA proteins). Indeed, the heptameric Bcs1 affords it the ability to create a larger entrance and substrate-binding cavity to accommodate the folded protein substrate.

Secondly, it seems that the binding cavity can only accommodate the substrate when all subunits of Bcs1 are in the apo or ADP-bound state, because in this conformation the substrate-binding cavity features an average diameter of 35 Å and a volume of 28 000 $Å^3$, which is large enough to contain the substrate. Our finding is in agreement with a prior observation showing that a strong interaction of ISP with Bcs1 only occurs in the absence of ATP [34]. The substrate-binding barrel is encircled by the AAA domains and by the seal-forming, Bcs1-specific domains that sharply narrow the barrel to a constriction of <5 Å in diameter, which is made of four hydrophobic residues (M121, M123, V124, and L128 of mouse sequence) arranged symmetrically from the seal loop of each subunit, separating the barrel from the TM basket. It is worth pointing out that the physiological relevance of the apo state is not clear because of the amount of ATP and ADP in the mitochondrial matrix. It is possible that the ADP form allows loading of substrate, which triggers subsequent nucleotide exchange. The observation that the presence of two different Apo conformations (Apo1 and Apo2) with different constriction sizes in the Bcs1-specific region may indicate that the pore opens and closes in a sort of breathing motion for Bcs1 in the absence of substrate. This could be possible as long as the membrane integrity is not compromised [31].

Thirdly, upon ATP binding, as seen from the ATPγS-bound structure, all Bcs1 subunits undergo, as proposed, a concerted conformational transition that shrinks the substrate-binding cavity to a volume of barely 9000 $Å^3$, reducing the cavity size by ~ 70%, so that it can no longer accommodate the substrate. Simultaneously, the opening to the cavity is reduced in diameter from 40 to 20 Å, preventing substrate from slipping back out of the cavity. Therefore, the ATPγS-bound structure represents the conformation of post-substrate translocation. It should also be mentioned that after the translocation, the substrate presumably remains bound to the Bcs1 via the TM helix and, possibly, the N-terminal segment [34], which is consistent with the model for Complex III assembly. Furthermore, in our ATPγS-bound structure, the pore dilates to a diameter of ~ 14 Å and is no longer plugged with the density of unknown identity. This 14 Å-diameter pore appears sufficient to accommodate the TM helix of the ISP.

Finally, hydrolysis of ATP by the Bcs1 subunits may achieve two objectives: one is rapid release of the TM helix of the substrate into the membrane section of Complex III, which suggests the possibility of opening the Bcs1 ring asymmetrically, and another is resetting the system back to the apo/ADP Bcs1 conformation, as represented by the postsubstrate release ADP-bound mBcs1 and yBcs1 structures and the apo mBcs1 structure.

Bcs1 represents a distinct class of AAA proteins

The assembly of Complex III is not the only process that requires transport of a folded protein across the membrane. In photosynthetic bacteria and in plant chloroplasts, the task of transporting folded proteins is designated to the Twin arginine translocation (Tat) pathway, a multi-subunit membrane protein complex coupling its function to membrane pmf [36]. Most interestingly, one substrate of the Tat system is the ISP subunit of the cyt b_6f complex, a homolog of the cyt bc_1 complex (Complex III) in plant chloroplasts [37]. Thus, researchers have speculated that over the

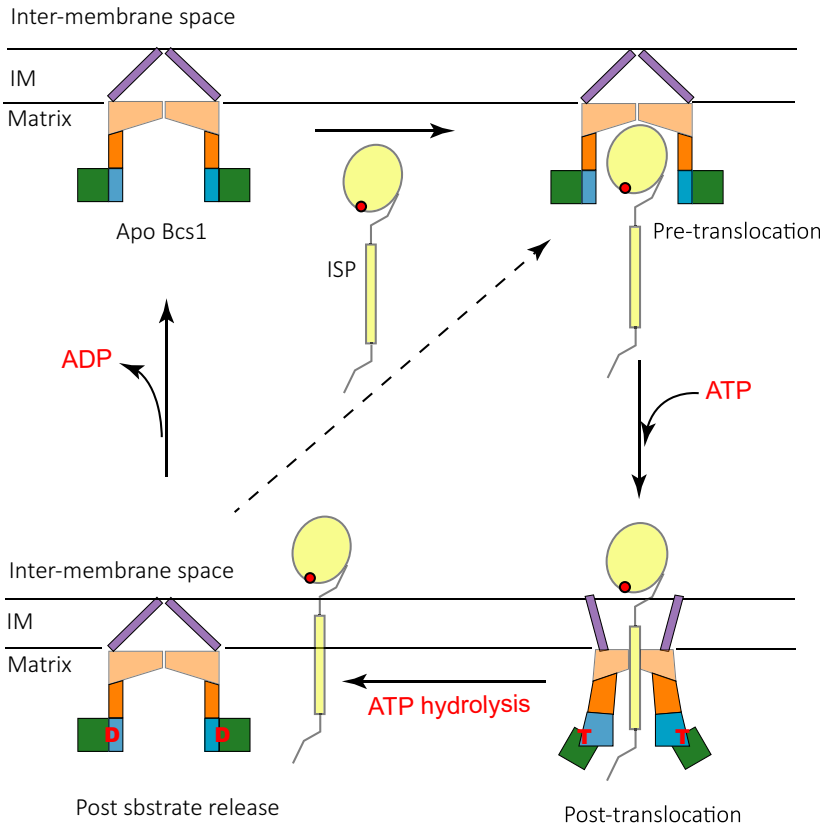

Fig. 4. Current model for the translocation of ISP by Bcs1. Two conformations of Bcs1 are presented schematically: Apo and ADP (D) conformation and ATP (T) conformation. Here, TM helices are colored in purple-blue, the Bcs1-specific domains in two different tones of orange, the AAA-L domain in green and the AAA-S domain in blue. The IM of mitochondria is shown as two black horizontal lines. The ISP is rendered with two domains: ISP-ED as a yellow oval and TM helix as a yellow rod. The 2Fe-2S cluster is depicted as a red dot. In the apo state, Bcs1 has a large entrance and cavity to hold the entire ISP-ED. Upon ATP binding, Bcs1 undergoes a very large conformational change that contracts the substrate-binding cavity and allows translocation of the ISP-ED across the mitochondrial IM. ATP hydrolysis releases ISP to the membrane section of Complex III and resets Bcs1 back to the apo conformation. The dashed diagonal line indicates that substrate binding could take place in the ADP state.

course of evolution Tat has been replaced by Bcs1 transporting folded proteins in mitochondria. It is worth pointing out that other systems exist in bacteria for transporting folded proteins. One well characterized example is the chaperone-user pathway, in which folded periplasmic pilin subunits are translocated across the outer membrane to form pili that are essential for bacterial pathogenesis [38].

Identical to other type I AAA proteins, Bcs1 has a functional, specialized domain at its N terminus and features a characteristic single AAA ATPase domain C-terminus to its subunit, which bears signature sequence motifs common to all AAA proteins. However, outside the core conserved AAA motifs such as Walker A and Walker B motifs, Bcs1 is quite different from other AAA proteins, displaying a low overall sequence identity (~ 30%). The difference is also shown in a phylogenetic analysis of AAA domain sequences, in which Bcs1 was grouped into its own clade [39]. The structures of mBcs1 and yBcs1 exhibit the following unique features that may be important to the function of this class of AAA proteins. First, the RecA-like domain of Bcs1 contains a 7-stranded β-sheet, in contrast to a 5-stranded β-sheet common to most AAA proteins. The extra two N-terminal β-strands connect to the Bcs1-specific domain. Second, the β-sheet II, or the connector hairpin, of the Bcs1-specific domain makes contact with the AAA domain of its neighboring subunit, indicating a communication pathway between neighboring subunits. Finally, ATP binding induces a sliding movement between neighboring AAA subunits such that the Arg-finger residues (R343 and R346) in the apo mBcs1 structure, which are 10 and 9 Å, respectively, away (Fig. 5A) from the superposed ATP in the ATP-bound structure, snap into position to make contact with the γ-phosphate of the bound ATPγS. For comparison, other AAA domains such as the bacterial σ54 activator NtrC1 and the D1 domain of protein unfoldase Cdc48/p97 show relatively small movements between neighboring subunits going from ATP to ADP states [40].

We propose that a unique, concerted transport mechanism may govern the function of Bcs1 based on the features revealed by the structures, which is in contrast to the more ubiquitous threading mechanism revealed by recent EM studies on a number of hexameric ring-shaped AAA proteins including the protein unfoldases p97 (Cdc48 in yeast) and Hsp104 [3,4,20], the DNA helicase [24], the proteasomal ATPase [21,22], the membrane fission Vps4 [41], and Rix 7 in

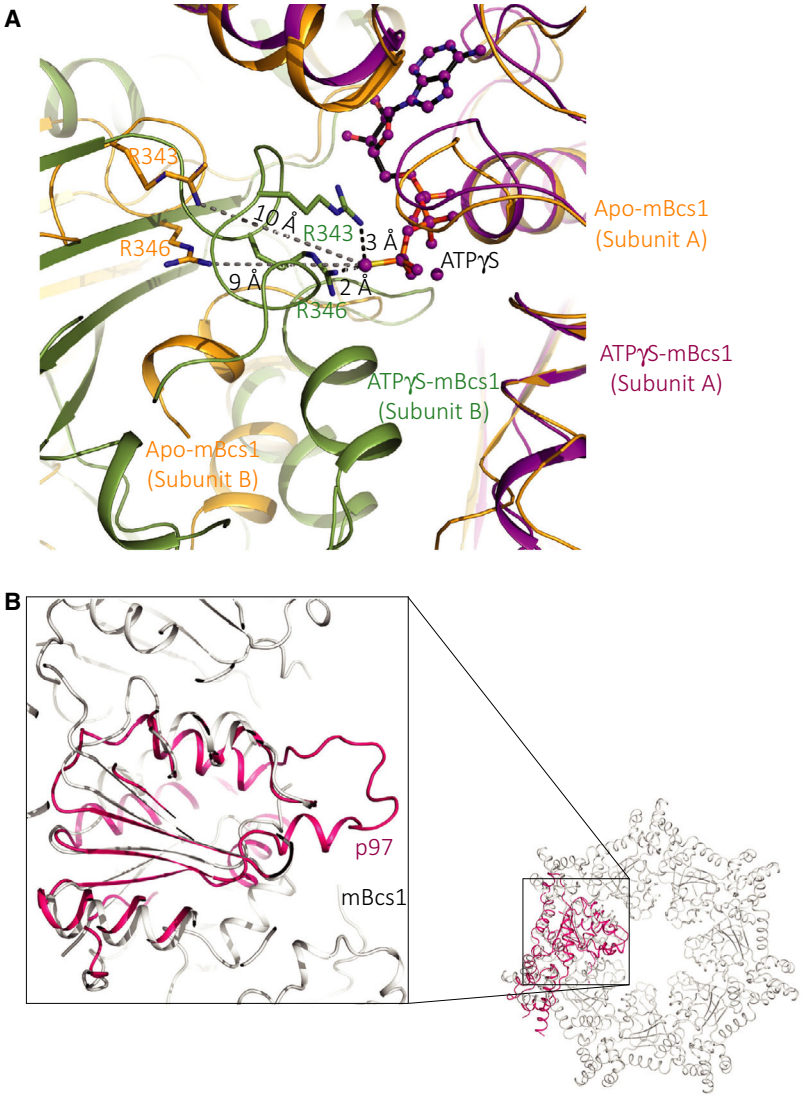

Fig. 5. Unique structural features of Bcs1. (A) Sliding movement at the interface of neighboring AAA domains. Upon ATP binding, AAA domains of mBcs1 undergo a sliding movement relative to its neighbor. Shown as cartoon in orange is the structure in the vicinity of the ATP-binding site for the apo structure (both subunits A and B), in which the Arg-finger residues R343 and R346 of subunit B of the apo mBcs1 are shown as stick models also in orange. Shown in magenta is the subunit A of the ATPγS-bound mBcs1 and in green is its neighboring subunit B. The Arg-finger residues R343 and R346 of subunit B of the ATPγS-bound structure are presented as stick models. The two structures are superimposed on the basis of subunit A. The distances from the side chain atoms NH2 of R343 and R346 of apo or ATPγS-bound Bcs1 to the γ-S atom of ATPγS are given. (B) One D2 subunit in red of p97 is superposed on the corresponding Bcs1 subunit in the heptameric context. Insect shows a portion of the superposition, demonstrating that the substrate-binding loop in p97 is missing in Bcs1.

ribosome assembly [42]. In those cases, protein substrates or DNA strands are dragged through a narrow channel formed by six AAA subunits. Mechanistically, in these AAA proteins, different nucleotide states simultaneously present in the six subunits of the hexamer coordinate with distinct spiral staircase-like arrangement of substrate-engaging pore loops in the central channel. The ATPase domains undergo a sequential, around-the-ring ATP hydrolysis cycle that leads to stepwise substrate translocation/dislocation.

Given the fact that Bcs1 belongs to the family of AAA proteins, we cannot rule out the possibility that Bcs1 uses a mechanism similar to the asymmetric hand-over-hand mechanism to transport the ISP-ED, especially considering the absence of substrate in current studies. That said, it is equally important to understand the roles of the distinct features in the AAA domain of Bcs1 in substrate translocation, which include Bcs1 forming its own clade in the phylogenetic tree, featuring a distinct 7-stranded β-sheet, and undergoing relatively large movements between subunits transitioning from apo to ATP states. Additionally, sequence alignment demonstrates that the AAA domain of Bcs1 is actually more similar to the D1 domain of p97/Cdc48, which does not appear to actively participate in substrate translocation. The D2 domain of p97/Cdc48, on the other hand, plays a major role in the hand-over-hand mechanism [3]. Moreover, the Bcs1 subunit lacks the critical substrate-contacting pore loop (Fig. 5B), one of the conserved structural motifs of those AAA ATPases that employ the hand-over-hand mechanism for threading. Also

missing in Bcs1 is the sensor-II region in the small helical domain that is known to involve in binding of ATP.

Structural comparison between mBcs1 and yBcs1

In the two recently published papers on the structures of Bcs1, a total of five EM structures and two crystal structures were presented (Table 1). Among these, three are EM structures for yBcs1, and two EM and two X-ray structures are for mBcs1, representing two dramatically different conformations and three nucleotide states. Because there is no equivalent structure of mBcs1 in the ATPγS-bound state for yBcs1, structural comparison was only conducted between apo-mBcs1 (PDB: 6UKP) and ADP-bound yBcs1 (PDB: 6SH3). Both structures were well determined at 3.8 and 3.4 Å resolution, respectively. Structure superposition for the entire heptamer supports the notion that apo mBcs1 and ADP-bound yBcs1 are in the same conformation due to a rms deviation of 3.5 Å for all aligned 2126 CA atoms using the molecular modeling program COOT [43]. Indeed, superposed yBcs1 in ADP-bound state and apo mBcs1 show the same pore size, the same volume of the substrate-binding cavity, and the same dimension for the entrance to the substrate-binding cavity. Structure-based sequence alignment of Bcs1 proteins from yeast and mouse gave a more accurate alignment with a sequence identity of 44% and similarity of 59%, respectively (Fig. 6A). The sequence similarity for the TM helix is limited compared to the Bcs1-specific and AAA domains.

Despite the overall good structural alignment, the TM helices do not superpose well, as TM helices of the apo mBcs1 are rotated counter-clockwise relative to those of ADP-bound yBcs1, when viewed along the 7-fold axis toward the matrix (Fig. 6B). Similar counter-clockwise rotation is also found for the seal-forming loops, as Bcs1 goes from the ADP-bound to the apo state, suggesting the possibility that these loops work like a camera diaphragm shutter, controlling the size of the pore. In addition to the rotation movement, there is an upward movement of the Bcs1 specific domain as the protein undergoes nucleotide state transition. Such an upward movement is also observed for the AAA domain. Thus, there is a coupling of the rotational and translational movement of each subunit during ADP to apo transition. The scale of this transition is likely magnified when Bcs1 is bound to ATP, leading to substrate translocation.

Structural interpretation of Bcs1 mutations that cause human diseases

Clinical investigations of patients with Complex III deficiencies have linked some cases to mutations in the gene *BCS1L*, which is the human bcs1 ortholog gene (bcs1-like gene). Presumably, mutants of Bcs1 fail the task to install the ISP subunit into the Complex III [27], leading to Complex III deficiency (MIM# 124000, www.omim.org) in neonates or infants with clinical presentation of encephalopathy alone or in combination with visceral involvement. However, it is puzzling that different mutations in Bcs1l result in a wide variety of clinical phenotypes that range from the relatively mild Björnstad syndrome to the severe GRACILE syndrome [44]. The GRACILE syndrome (MIM# 603358, Growth Retardation, Aminoaciduria, Cholestasis, Iron overload, Lactacidosis, and Early death) is a severe form of the disease that results in liver and kidney failure in young children. By contrast, the Björnstad syndrome (MIM# 262000) has a much milder clinical presentation with patients showing highly restricted pili torti (twisted hair) and sensorineural hearing loss [45]. Curiously, Björnstad syndrome-causing mutations are accompanied by increased level of reactive oxygen species (ROS) [46]. In real life, clinical presentations of *BCS1L* mutations can fall anywhere between the two extremes [47].

Table 1. Structural models of Bcs1 in the PDB.

PDB	Organism	Construct (no. residues)	Method	Nucleotide state	Overall map. resolution (Å)	Model	Ref
6UKP	Mouse	Full-length (1–418)	EM	Apo	3.8	29–417	[30]
6UKS	Mouse	Full–length (1–418)	EM	ATPγS	3.2	49–418	[30]
6U1Y	Mouse	AAA domain (151–418)	X-ray	AMP-PNP	2.2	164–418	[30]
6UKO	Mouse	Full-length (1–418)	X-ray	ADP	4.4	49–417	[30]
6SH3	Yeast	Full-length (1–456)	EM	ADP	3.4	49–449	[31]
6SH4	Yeast	Full-length (1–456)	EM	Apo1	4.4	49–449 (No side chain)	[31]
6SH5	Yeast	Full-length (1–456)	EM	Apo2	4.6	84–449 (No side chain)	[31]

A

```
YEAST   1    MSDKPIDIQYDKQATPNLSGVITPPTNKIDNDSVR 35

Mouse   1    MPFSDFVLALKDNPYFGAGFGLVGVGTALAMARKGAQLGLVAFRRHYMITLEVPA-RDRSY  60
Yeast  36    EKLSKLVGDAMSNNPYFAAGGGLMILGTGLAVARSGIIKASRVLYRQMIVDLEIQSKDKSY  96

Mouse   61   AWLLSWLTRHSTR-TQHLSVETSYLQHESGRISTKFEFIPSPGNHFIWYQGKWIRVERNRD  120
Yeast   97   AWFLTWMAKHPQRVSRHLSVRTNYIQHDNGSVSTKFSLVPGPGNHWIRYKGAFILIKRERS  157

Mouse   121  MQMVDLQTGTPWESVTFTALGTDRKVFFNILEEARALALQQEEGKTVMYTAVGSEWRTFG  180
Yeast   158  AKMIDIANGSPFETVTLTTLYRDKHLFDDILNEAKDIALKTTEGKTVIYTSFGPEWRKFG  217

Mouse   181  YPRRRRPLDSVVLQQGLADRIVKDIREFIDNPKWYIDRGIPYRRGYLLYGPPGCGKSSFI  240
YEAST   218  QPKAKRMLPSVILDSGIKEGILDDVYDFMKNGKWYSDRGIPYRRGYLLYGPPGSGKTSFI  277

Mouse   241  TALAGELEHSICLLSLTDSSLSDDRLNHLLSVAPQQSLVLLEDVDAAFLSRD-LAVENPIK  300
Yeast   278  QALAGELDYNICILNLSENNLTDDRLNHLMNNMPERSILLLEDIDAAFNKRS--QTGEQ-G  335

Mouse   301  YQGLGRLTFSGLLNALDGVASTEARIVFMTTNYIDRLDPALIRPGRVDLKEYVGYCSHWQ  360
Yeast   336  FHS--SVTFSGLLNALDGVTSSEETITFMTTNHPEKLDAAIMRPGRIDYKVFVGNATPYQ  393

Mouse   361  LTQMFQRFYPGQ-APSLAENFAEHVLKATSEISPAQVQGYFMLYKNDPMGAVHNIESLR  418
Yeast   394  VEKMFMKFYPGETDICKKFVNSVK--ELDITVSTAQLQGLFVMNKDAPHDALKMVSSLRNANHIF 456
```

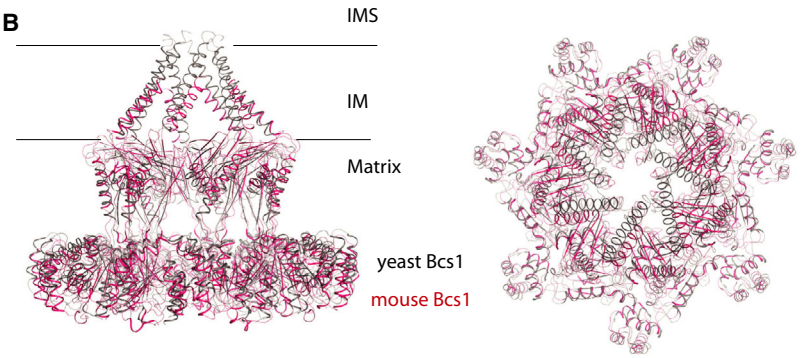

Fig. 6. Comparison of mouse and yeast Bcs1. (A) Structure-based sequence alignment between mBcs1 and yBcs1. In the alignment, conserved residues are shown as boldfaced characters and similar residues are colored green. (B) Superposition of the mouse Bcs1 (red) in the apo state and yeast Bcs1 (gray) in the ADP-bound state. Superposed structures are shown in cartoons in two orthogonal orientations.

Diseases caused by *BCS1L* mutations are autosomal recessive, requiring both copies to be mutated. Positively charged residues, mostly arginine residues, are involved in 60% of missense mutations. Furthermore, many of the mutated residues are highly conserved. Studies on the phenotype-genotype relationship have primarily focused on mapping *BCS1L* mutations to structural models of Bcs1l [46,47]. These studies faced difficulties in the use of structures created by homology modeling, which we are now able to overcome by using experimental structures of mBcs1. The structure of mouse Bcs1 is an excellent representation of human Bcs1 structure, because they share 94% sequence identity. By mapping 2D sequence locations of the mutations onto the 3D structure of mBcs1, we were able to establish a correlation between the 3D positions of the mutations and the reported severity of symptoms displayed by patients. For example, we found that GRACILE syndrome is often seen in patients with mutations in the Bcs1-specific domains, whereas the milder Björnstad syndrome links more frequently to mutations in the AAA domain. Thus, structural analysis suggests a relationship between the severity in clinical presentation or prognosis of *BCS1L* mutations and the structural integrity of various regions of the protein. Because the Bcs1-specific region may work as a seal or shutter to control substrate passage through the membrane and may play an essential role in preventing harmful dissipation of membrane pmf during the translocation process, it seems reasonable that mutations in this region result in more severe consequence. By contrast, the AAA domain mutations may only cause problem in the assembly of Complex III, which seems consistent with the observation that these mutations often lead to increased production of ROS due to increased pmf [46].

Conclusions and Future directions

Having determined the structures of mBcs1 and yBcs1 in different nucleotide states and conformations, we now have acquired a structural framework from which more detailed mechanistic insights into the transport function of Bcs1 can be expected. Future studies will likely reveal how Bcs1 recognizes and binds the folded ISP-ED, capture its action in transporting the ISP substrate across the membrane, and witness how substrate is released into the membrane. To achieve these goals, a combination of various research approaches will have to be used.

From a structural point of view, it is necessary to obtain the structure of Bcs1 in complex with the substrate ISP in order to address the questions on how substrate binding trigger changes in Bcs1 and whether binding of substrate is sufficient to induce nucleotide exchange. Structures are also needed to determine whether subunits of Bcs1 functions in a sequential fashion or in a concerted manner. The former is the hallmark of the hand-over-hand or split wash mechanism of translocation displayed by many hexameric AAA proteins. In the apo and ADP-bound structures, the unknown density plugging the small pore in the center of the Bcs1-specific domains should also be investigated.

Biochemically, kinetic study of the life span of different nucleotide states will provide clues on the rate limiting steps in the reaction landscape. Coupling these studies with mutagenesis will likely play a major role in verifying various mechanistic hypotheses. For example, to prevent proton leakage during translocation, an airlock-like mechanism was proposed [31]. However, how the opening and closure of the seal pore is controlled requires further elucidation. Mutagenesis studies will allow functional and structural characterizations of many documented disease-related mutants. The structures should also facilitate development of drugs to modulate function of Bcs1.

Acknowledgements

This research was supported by the Intramural Research Program (Z01 Number: ZIA BC 010600) of the Center for Cancer Research (CCR), National Cancer Institute (NCI), National Institutes of Health (NIH). The EM work is assisted by the NIH Intramural Cryo-EM (NICE) facility, by the Center for Molecular Microscopy (CMM) and by the NIH Biowulf high performance computing center. The author also thanks George Leiman for editorial assistance.

Conflict of interest

The authors declare no conflict of interest.

Peer Review

The peer review history for this article is available at https://publons.com/publon/10.1111/febs.15576.

References

1 Rapoport TA, Li L & Park E (2017) Structural and Mechanistic Insights into Protein Translocation. *Annu Rev Cell Dev Biol* **33**, 369–390.

2 Chacinska A, Koehler CM, Milenkovic D, Lithgow T & Pfanner N (2009) Importing mitochondrial proteins: machineries and mechanisms. *Cell* **138**, 628–644.

3 Twomey EC, Ji Z, Wales TE, Bodnar NO, Ficarro SB, Marto JA, Engen JR & Rapoport TA (2019) Substrate processing by the Cdc48 ATPase complex is initiated by ubiquitin unfolding. *Science* **365**, eaax1033.

4 Cooney I, Han H, Stewart MG, Carson RH, Hansen DT, Iwasa JH, Price JC, Hill CP & Shen PS (2019) Structure of the Cdc48 segregase in the act of unfolding an authentic substrate. *Science* **365**, 502–505.

5 Xia D, Yu CA, Kim H, Xia JZ, Kachurin AM, Zhang L, Yu L & Deisenhofer J (1997) Crystal structure of the cytochrome bc1 complex from bovine heart mitochondria. *Science* **277**, 60–66.

6 Hunte C, Koepke J, Lange C, Rossmanith T & Michel H (2000) Structure at 2.3 A resolution of the cytochrome bc(1) complex from the yeast *Saccharomyces cerevisiae* co-crystallized with an antibody Fv fragment. *Structure* **15**, 669–684.

7 Esser L, Yu CA & Xia D (2014) Structural basis of resistance to anti-cytochrome bc(1) complex inhibitors: implication for drug improvement. *Curr Pharm Des* **20**, 704–724.

8 DiMauro S & Schon EA (2003) Mitochondrial respiratory-chain diseases. *N Engl J Med* **348**, 2656–2668.

9 Pfanner N, Warscheid B & Wiedemann N (2019) Mitochondrial proteins: from biogenesis to functional networks. *Nat Rev Mol Cell Biol* **20**, 267–284.

10 Cui TZ, Smith PM, Fox JL, Khalimonchuk O & Winge DR (2012) Late-stage maturation of the Rieske Fe/S protein: Mzm1 stabilizes Rip1 but does not facilitate its translocation by the AAA ATPase Bcs1. *Mol Cell Biol* **32**, 4400–4409.

11 Wagener N & Neupert W (2012) Bcs1, a AAA protein of the mitochondria with a role in the biogenesis of the respiratory chain. *J Struct Biol* **179**, 121–125.

12 Esser L, Gong X, Yang S, Yu L, Yu CA & Xia D (2006) Surface-modulated motion switch: capture and release of iron-sulfur protein in the cytochrome bc1 complex. *Proc Natl Acad Sci USA* **103**, 13045–13050.

13 Tian H, Yu L, Mather MW & Yu CA (1998) Flexibility of the neck region of the rieske iron-sulfur protein is functionally important in the cytochrome bc1 complex. *J Biol Chem* **273**, 27953–27959.

14 Lill R (2009) Function and biogenesis of iron-sulphur proteins. *Nature* **460**, 831–838.

15 Graham LA, Brandt U, Sargent JS & Trumpower BL (1993) Mutational analysis of assembly and function of the iron-sulfur protein of the cytochrome bc1 complex in *Saccharomyces cerevisiae*. *J Bioenerg Biomembr* **25**, 245–257.

16 Brandt U, Yu L, Yu CA & Trumpower BL (1993) The mitochondrial targeting presequence of the Rieske iron-

sulfur protein is processed in a single step after insertion into the cytochrome bc1 complex in mammals and retained as a subunit in the complex. *J Biol Chem* **268**, 8387–8390.
17 Cruciat CM, Hell K, Folsch H, Neupert W & Stuart RA (1999) Bcs1p, an AAA-family member, is a chaperone for the assembly of the cytochrome bc(1) complex. *EMBO J* **18**, 5226–5233.
18 Nobrega FG, Nobrega MP & Tzagoloff A (1992) BCS1, a novel gene required for the expression of functional Rieske iron-sulfur protein in *Saccharomyces cerevisiae*. *EMBO J* **11**, 3821–3829.
19 Ogura T & Wilkinson AJ (2001) AAA+ superfamily ATPases: common structure–diverse function. *Genes Cells* **6**, 575–597.
20 Gates SN, Yokom AL, Lin J, Jackrel ME, Rizo AN, Kendsersky NM, Buell CE, Sweeny EA, Mack KL, Chuang E *et al*. (2017) Ratchet-like polypeptide translocation mechanism of the AAA+ disaggregase Hsp104. *Science* **357**, 273–279.
21 de la Pena AH, Goodall EA, Gates SN, Lander GC & Martin A (2018) Substrate-engaged 26S proteasome structures reveal mechanisms for ATP-hydrolysis-driven translocation. *Science* **362**, eaav0725.
22 Dong Y, Zhang S, Wu Z, Li X, Wang WL, Zhu Y, Stoilova-McPhie S, Lu Y, Finley D & Mao Y (2019) Cryo-EM structures and dynamics of substrate-engaged human 26S proteasome. *Nature* **565**, 49–55.
23 Itskanov S & Park E (2019) Structure of the posttranslational Sec protein-translocation channel complex from yeast. *Science* **363**, 84–87.
24 Gao Y, Cui Y, Fox T, Lin S, Wang H, de Val N, Zhou ZH & Yang W (2019) Structures and operating principles of the replisome. *Science* **363**, eaav7003.
25 Folsch H, Guiard B, Neupert W & Stuart RA (1996) Internal targeting signal of the BCS1 protein: a novel mechanism of import into mitochondria. *EMBO J* **15**, 479–487.
26 Petruzzella V, Tiranti V, Fernandez P, Ianna P, Carrozzo R & Zeviani M (1998) Identification and characterization of human cDNAs specific to BCS1, PET112, SCO1, COX15, and COX11, five genes involved in the formation and function of the mitochondrial respiratory chain. *Genomics* **54**, 494–504.
27 De Meirleir L, Seneca S, Damis E, Sepulchre B, Hoorens A, Gerlo E, Garcia Silva MT, Hernandez EM, Lissens W & Van Coster R (2003) Clinical and diagnostic characteristics of complex III deficiency due to mutations in the BCS1L gene. *Am J Med Genet A* **121A**, 126–131.
28 Fernandez-Vizarra E, Bugiani M, Goffrini P, Carrara F, Farina L, Procopio E, Donati A, Uziel G, Ferrero I & Zeviani M (2007) Impaired complex III assembly associated with BCS1L gene mutations in isolated mitochondrial encephalopathy. *Hum Mol Genet* **16**, 1241–1252.
29 Ostojic J, Rago JP & Dujardin G (2014) A novel mechanism involved in the coupling of mitochondrial biogenesis to oxidative phosphorylation. *Microb Cell* **1**, 43–44.
30 Tang WK, Borgnia MJ, Hsu AL, Esser L, Fox T, de Val N & Xia D (2020) Structures of AAA protein translocase Bcs1 suggest translocation mechanism of a folded protein. *Nat Struct Mol Biol* **27**, 202–209.
31 Kater L, Wagener N, Berninghausen O, Becker T, Neupert W & Beckmann R (2020) Structure of the Bcs1 AAA-ATPase suggests an airlock-like translocation mechanism for folded proteins. *Nat Struct Mol Biol* **27**, 142–149.
32 Holm L & Sander C (1993) Protein structure comparison by alignment of distance matrices. *J Mol Biol* **233**, 123–138.
33 Nouet C, Truan G, Mathieu L & Dujardin G (2009) Functional analysis of yeast bcs1 mutants highlights the role of Bcs1p-specific amino acids in the AAA domain. *J Mol Biol* **388**, 252–261.
34 Wagener N, Ackermann M, Funes S & Neupert W (2011) A pathway of protein translocation in mitochondria mediated by the AAA-ATPase Bcs1. *Mol Cell* **44**, 191–202.
35 Gao X, Wen X, Yu C, Esser L, Tsao S, Quinn B, Zhang L, Yu L & Xia D (2002) The crystal structure of mitochondrial cytochrome bc1 in complex with famoxadone: the role of aromatic-aromatic interaction in inhibition. *Biochemistry* **41**, 11692–11702.
36 Palmer T & Berks BC (2012) The twin-arginine translocation (Tat) protein export pathway. *Nat Rev Microbiol* **10**, 483–496.
37 Kurisu G, Zhang H, Smith JL & Cramer WA (2003) Structure of the cytochrome b6f complex of oxygenic photosynthesis: tuning the cavity. *Science* **302**, 1009–1014.
38 Busch A & Waksman G (2012) Chaperone-usher pathways: diversity and pilus assembly mechanism. *Philos Trans R Soc Lond B Biol Sci* **367**, 1112–1122.
39 Frickey T & Lupas AN (2004) Phylogenetic analysis of AAA proteins. *J Struct Biol* **146**, 2–10.
40 Tang WK, Li D, Li CC, Esser L, Dai R, Guo L & Xia D (2010) A novel ATP-dependent conformation in p97 N-D1 fragment revealed by crystal structures of disease-related mutants. *EMBO J* **29**, 2217–2229.
41 Han H, Monroe N, Sundquist WI, Shen PS & Hill CP (2017) The AAA ATPase Vps4 binds ESCRT-III substrates through a repeating array of dipeptide-binding pockets. *Elife* **6**, e31324.
42 Lo YH, Sobhany M, Hsu AL, Ford BL, Krahn JM, Borgnia MJ & Stanley RE (2019) Cryo-EM structure of the essential ribosome assembly AAA-ATPase Rix7. *Nat Commun* **10**, 513.

43 Emsley P & Cowtan K (2004) Coot: model-building tools for molecular graphics. *Acta Crystallogr D Biol Crystallogr* **60**, 2126–2132.
44 Moran M, Marin-Buera L, Gil-Borlado MC, Rivera H, Blazquez A, Seneca S, Vazquez-Lopez M, Arenas J, Martin MA & Ugalde C (2010) Cellular pathophysiological consequences of BCS1L mutations in mitochondrial complex III enzyme deficiency. *Hum Mutat* **31**, 930–941.
45 Ramos-Arroyo MA, Hualde J, Ayechu A, De Meirleir L, Seneca S, Nadal N & Briones P (2009) Clinical and biochemical spectrum of mitochondrial complex III deficiency caused by mutations in the BCS1L gene. *Clin Genet* **75**, 585–587.
46 Hinson JT, Fantin VR, Schonberger J, Breivik N, Siem G, McDonough B, Sharma P, Keogh I, Godinho R, Santos F *et al*. (2007) Missense mutations in the BCS1L gene as a cause of the Bjornstad syndrome. *N Engl J Med* **356**, 809–819.
47 Baker RA, Priestley JRC, Wilstermann AM, Reese KJ & Mark PR (2019) Clinical spectrum of BCS1L Mitopathies and their underlying structural relationships. *Am J Med Genet A* **179**, 373–380.